Bioscience, Biotechnology, and Biochemistry, 2021, Vol. 85, No. 1, 168-180

doi: 10.1093/bbb/zbaa024
Advance access publication date: 7 January 2021
REGULAR PAPER

REGULAR PAPER

Effects of side chain length of 10-methyl-aplog-1, a simplified analog of debromoaplysiatoxin, on PKC binding, anti-proliferative, and pro-inflammatory activities

Atsuko Gonda,[1] Koji Takada,[1] Ryo C. Yanagita,[2] Shingo Dan,[3] and Kazuhiro Irie [1,*]

[1]Division of Food Science and Biotechnology, Graduate School of Agriculture, Kyoto University, Kyoto, Japan; [2]Department of Applied Biological Science, Faculty of Agriculture, Kagawa University, Kagawa, Japan; and [3]Division of Molecular Pharmacology, Cancer Chemotherapy Center, Japanese Foundation for Cancer Research, Tokyo, Japan

*Correspondence: Kazuhiro Irie, irie.kazuhiro.2z@kyoto-u.ac.jp

ABSTRACT

10-Methyl-aplog-1 (**1**), a simplified analog of debromoaplysiatoxin, exhibits a high binding affinity for protein kinase C (PKC) isozymes and potent antiproliferative activity against several cancer cells with few adverse effects. A recent study has suggested that its phenol group in the side chain is involved in hydrogen bonding and CH/π interactions with the binding cleft-forming loops in the PKCδ-C1B domain. To clarify the effects of the side chain length on these interactions, four analogs of **1** with various lengths of side chains (**2-5**) were prepared. The maximal PKC binding affinity and antiproliferative activity were observed in **1**. Remarkably, the introduction of a bromine atom into the phenol group of **2** increased not only these activities but also proinflammatory activity. These results indicated that **1** has the optimal side chain length as an anticancer seed. This conclusion was supported by docking simulations of **1-5** to the PKCδ-C1B domain.

Graphical Abstract

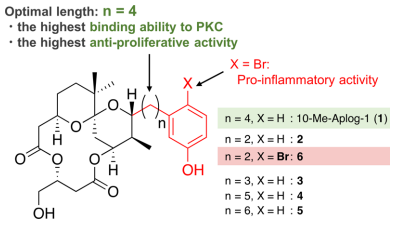

Received: 10 August 2020; **Accepted:** 22 August 2020

Optimal length of the side chain linker was four ($n = 4$) regarding desired biological activities. A bromine atom on the aromatic ring provided proinflammatory activity.

Keywords: antiproliferative, cancer, debromoaplysiatoxin, protein kinase C, tumor promoter

Abbreviations: AIDS: acquired immunodeficiency syndrome; ATX: aplysiatoxin; bryo-1: bryostatin-1; DAT: debromoaplysiatoxin; MD: molecular dynamics; MM-PBSA: molecular mechanics Poisson–Boltzmann surface area; MG-MID: mean-graph midpoint value; PDBu: phorbol 12,13-dibutylate; PKC: protein kinase C; TPA: 12-*O*-tetradecanoylphorbol 13-acetate

Protein kinase C isozymes (PKCs) are serine/threonine kinases involved in intracellular signal transduction and are closely associated with cell proliferation, differentiation, and apoptosis (Nishizuka 1986). PKCs consist of at least 10 isozymes in humans, which are classified into 3 subfamilies based on the characteristics of their regulatory domains: conventional PKCs (α, βI, βII, γ), novel PKCs (δ, ε, θ, η), and atypical PKCs (ζ, λ) (Nishizuka 1995; Steinberg 2008). These isozymes are one of the promising therapeutic target enzymes to treat intractable diseases such as cancer, Alzheimer's disease, and acquired immunodeficiency syndrome (AIDS) (Nelson and Alkon 2009; Andersen *et al.* 2018; Isakov 2018). Activation of PKCs is a promising strategy for treatments of cancer because recent investigations have suggested that many cancer cells had loss-of-function mutations in PKCs, indicating that the activation of PKCs could lead to the suppression of tumor growth (Antal *et al.* 2015).

Naturally occurring PKC activators like 12-*O*-tetradecanoylphorbol 13-acetate (TPA), teleocidin B-4, and aplysiatoxin (ATX) are well-known tumor promoters (Figures 1 and 2; Fujiki and Sugimura 1987). These compounds activate PKCs (Fujiki *et al.* 1984) by binding to their C1 domains (Ono *et al.* 1989). Following binding of these compounds to the C1 domains, PKCs localize to cellular membrane compartments, where they transition to the fully activated state and undergo downregulation (Antal and Newton 2014). While 1,2-*sn*-diacylglycerol, an endogenous PKC activator, is quickly metabolized after activation of PKCs, tumor promoters persist for a longer time period in cells and maintain PKCs in the activated state for a longer time (Nishizuka 1992). This process induces the down-regulation of PKCs via the ubiquitin-proteasome pathway, leading to tumor promotion as PKCs act as tumor suppressors (Antal *et al.* 2015).

There are PKC activators with minimal proinflammatory and tumor-promoting activities. Bryostatin-1 (bryo-1), which was isolated from a marine bryozoan *Bugula neritina* (Figure 1) (Pettit *et al.* 1982), is a potent activator of PKCs without these adverse effects (Mutter and Wills 2000). Bryo-1 has been clinically tested in phase I and II trials as a promising chemotherapeutic agent, but it has not been applied clinically as chemotherapy (Kollár *et al.* 2014). On the other hand, bryo-1 is under phase II clinical trial investigation for treatment of Alzheimer's disease (Russo *et al.* 2016) and has been investigated as a latency-reversing agent (LRA) to potentially eradicate human immunodeficiency virus (HIV) infections (Gutiérrez *et al.* 2016).

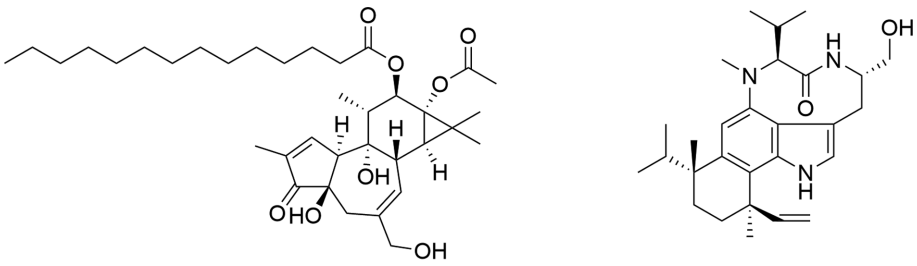

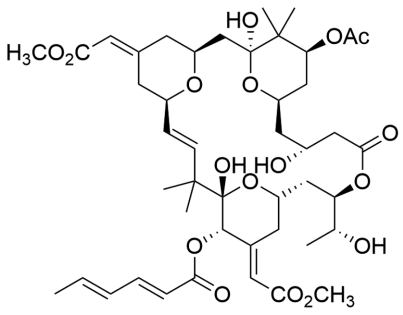

Figure 1. Structure of natural protein kinase C (PKC) activators.

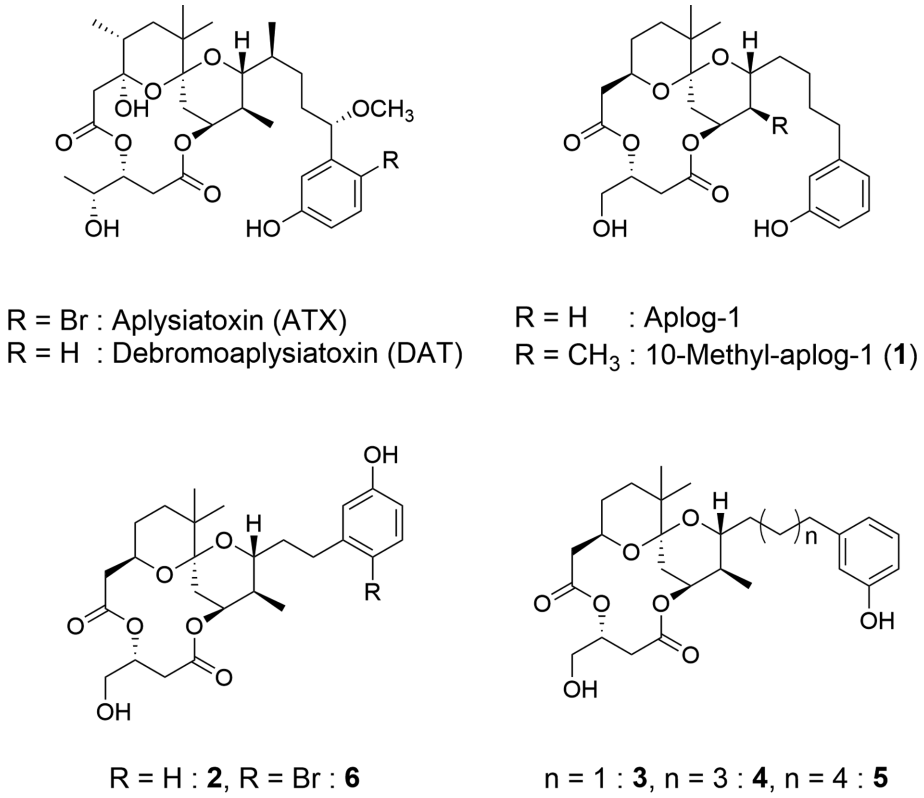

Figure 2. Structure of aplog-1, 10-methyl-aplog-1 (**1**), and its derivatives (**2-6**).

ATX and debromoaplysiatoxin (DAT) were isolated from *Stylocheilus longicauda* by Kato and Scheuer (1974) as potent proinflammatory agents with macrolactone structures that resemble bryo-1 (Figure 2). ATX, which is more hydrophobic (log $P = 5.4$) (Kamachi *et al.* 2013) than bryo-1 (log $P = 2.9$) (Bignami *et al.* 1996), exhibited potent tumor-promoting activity *in vivo* (Suganuma *et al.* 1984). On the other hand, the tumor-promoting and related activities of DAT (log $P = 4.4$) were significantly weaker than those of ATX, though their binding affinities to PKCs were almost equivalent (Shimomura *et al.* 1983; Suganuma *et al.* 1984). The hydrophobicity of a bromine atom is considered to play an important role in the tumor-promoting activity of ATX (Kishi and Rando 1998). Based on the importance of hydrophobicity in the adverse effects of ATX and DAT, aplog-1 was developed as a simplified, stabilized, and less hydrophobic analog of DAT in our laboratory as a surrogate of bryo-1 (Figure 2; Nakagawa *et al.* 2009). Aplog-1 bound to PKCδ with a K_i value of 15 nM, but exhibited limited tumor-promoting related activities (Nakagawa *et al.* 2009; Irie *et al.* 2012). It also inhibited the growth of several cancer cell lines, suggesting that it has potential as a new lead compound for cancer chemotherapy. Comprehensive structure-activity studies on the spiroketal moiety of aplog-1 identified 10-methyl-aplog-1 (**1**) to be one order of magnitude more potent than aplog-1 as a PKC binder and to show potent antiproliferative activities similar to those of DAT, but with limited proinflammatory and tumor-promoting activities (Kikumori *et al.* 2012; Kikumori *et al.* 2016).

Structure-activity studies on the side chain with a phenol moiety of **1** were also investigated (Kamachi *et al.* 2013; Hanaki *et al.* 2017). The introduction of various substituents into the phenol moiety suggested that antiproliferative and PKC binding activities correlated with the hydrophobicity of the molecule and that the maximal activities were found at a log P value of 4.0-4.5 (Kamachi *et al.* 2013). Other research in our laboratory revealed that the aromatic ring and the phenolic hydroxy group on the side chain of **1** were involved in the interaction with the C1B domain of PKCδ through hydrogen bonding or CH/π interactions, which could reduce the side effects (Hanaki *et al.* 2017). However, the effects of side chain length on the activities of **1** have not yet been investigated. The purpose of this study is to clarify the effects of the side chain length of **1** on these interactions with PKCs and various biological activities including PKC binding, antiproliferative, and proinflammatory activities. Here, we describe the syntheses of five analogs of **1** with various side chain lengths (**2-6**) and their biological evaluation (Figure 2).

Results and discussion

Synthesis of the derivatives of 1 (2-6)

The side chain length of 10-methyl-aplog-1 (**1**) was changed systematically as shown in Figure 2 (**2-5**). Compounds **2** and **3** have shorter alkyl chains than **1**, and **4** and **5** have longer ones. The retrosynthetic analyses of **2-5** are shown in Scheme 1. They were synthesized by the previously reported convergent route (Kikumori *et al.* 2012) from the corresponding epoxide units (**A-D**), the carboxylic acid unit (**E**), and the dithiane unit (**F**).

At first, 4 aldehydes (**10**, **11**, **15**, and **16**) were synthesized by conventional methods as shown in Scheme 2. Methyl 3-(3-benzyloxyphenyl)propionate (**7**) and methyl (3-benzyloxyphenyl)acetate (**12**) were used as the starting materials for each synthesis. Extension of 2 carbons was performed by a cycle of $LiAlH_4$ reduction, bromination, diethyl malonate condensation, and Krapcho decarboxylation. Brown's diastereoselective crotylation (Brown and Bhat 1986) of each aldehyde gave

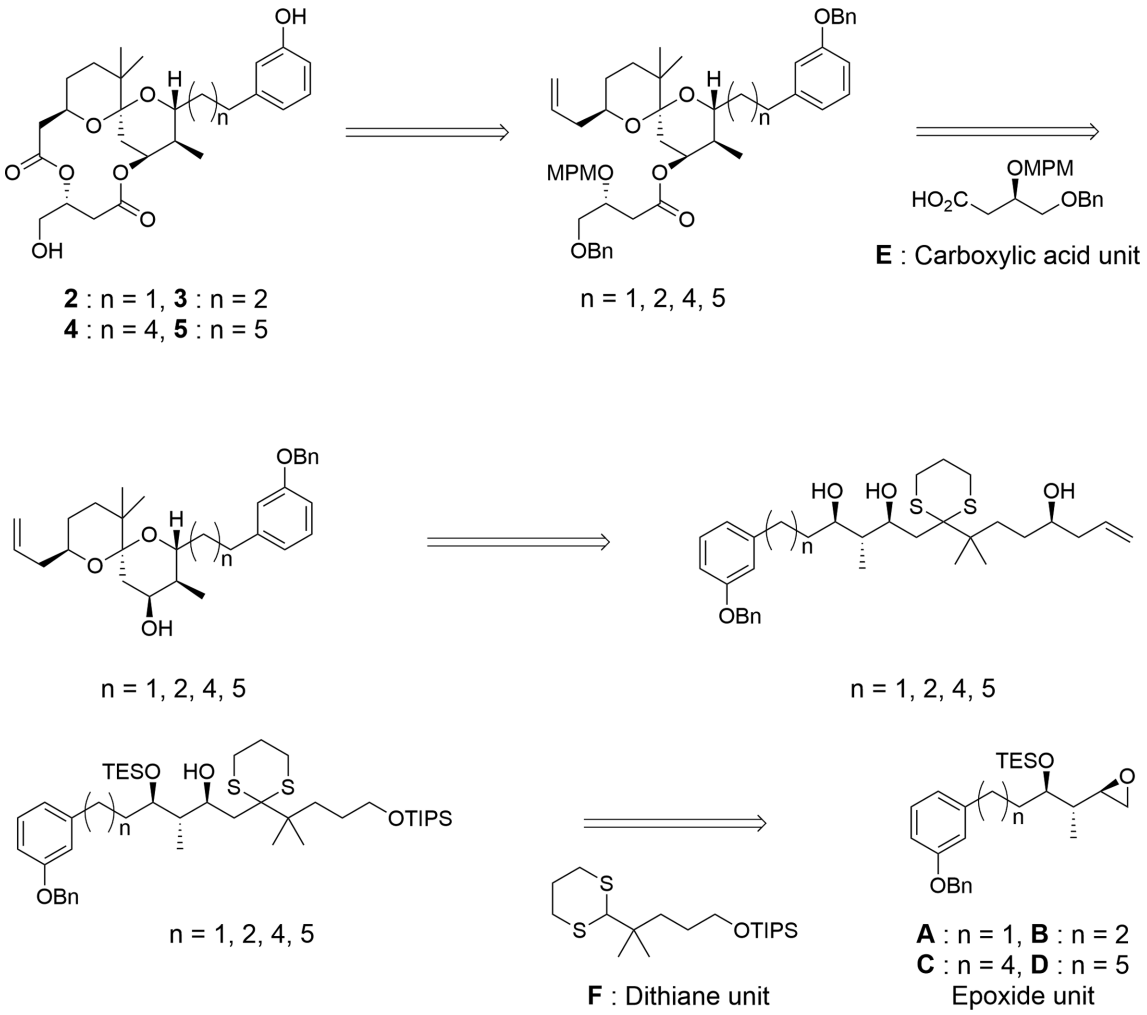

Scheme 1. The retrosynthetic analyses of **2**-**5**.

the desired homoallylic alcohols with diastereomeric excess of 75-90% (Supplemental Material). The undesired diastereomers were completely separated by silica gel column chromatography after the next epoxidation reaction. The homoallylic alcohols were treated with *tert*-butyl hydroperoxide and a catalytic amount of vanadyl acetylacetonate to give the desired epoxides whose hydroxy groups were then protected as triethylsilyl (TES) ethers to give **A-D**. The enantiomeric excess of each epoxide (**SI1**, **SI5**, **SI9**, and **SI16**) was estimated to be 89-91% by HPLC using a chiral column (CHIRALCEL OJ-RH; Supplemental Material).

The synthesis of **2** is shown as a representative example in Scheme 3. The synthesis of **3-5** is summarized in Supplemental Material (Schemes SI-1-SI-3). The coupling of **A** with the known dithiane **F** (Nakagawa *et al.* 2009), followed by deprotection of the TES group, gave a diol which was then protected as an acetonide (**21**). Parikh–Doering oxidation (Parikh and Doering 1967) of **21** followed by Maruoka's asymmetric allylation (Hanawa *et al.* 2003) yielded a homoallylic alcohol, whose acetonide group was then cleaved by acidic hydrolysis. The deprotection of the dithiane group in the resultant triol (**22**) by Selectfluor™ (Liu and Wong 2002) gave a desired single anomeric spiroketal (**23**) in moderate yield. The configuration of the spiroketal moiety was determined by the method reported previously (Kikumori *et al.* 2012; Kikumori *et al.* 2016) using nuclear Overhauser enhancement.

Yamaguchi's esterification (Inanaga *et al.* 1979) of **23** with the carboxylic acid unit **E** yielded an ester, whose 4-methoxyphenylmethyl (MPM) group was then deprotected by 2,3-dichloro-5,6-dicyano-*p*-benzoquinone (DDQ) to give **24**. After oxidative cleavage of the terminal alkene, macrolactonization was performed by Yamaguchi's method (Inanaga *et al.* 1979). Compound **2** was obtained by catalytic hydrogenolysis of the resultant macrolactone. Bromination of **2** using benzyltrimethylammonium tribromide (Kajigaeshi *et al.* 1987) gave **6**. The total yield of **2** was 2.3%, achieved through 16 steps. Yields of **3-5** were 0.26% through 20 steps, 0.11% through 24 steps, and 1.3% through 24 steps, respectively (Supplemental Material).

Ability of 2-6 to bind to PKC-C1 domains

We recently identified the PKC isozymes (PKCα and δ) involved in the anti-proliferative and pro-apoptotic activities of **1** in several cancer cell lines (Hanaki *et al.* 2018). We thus evaluated the binding affinity to PKCα-C1A and δ-C1B by a competitive binding assay using [^{3}H]phorbol 12,13-dibutylate (PDBu) (Sharkey and Blumberg 1985). We used PKC C1 peptides that were chemically synthesized and folded by zinc treatment (Irie *et al.* 1998; Shindo *et al.* 2001). It has been confirmed that natural PKC ligands bind to

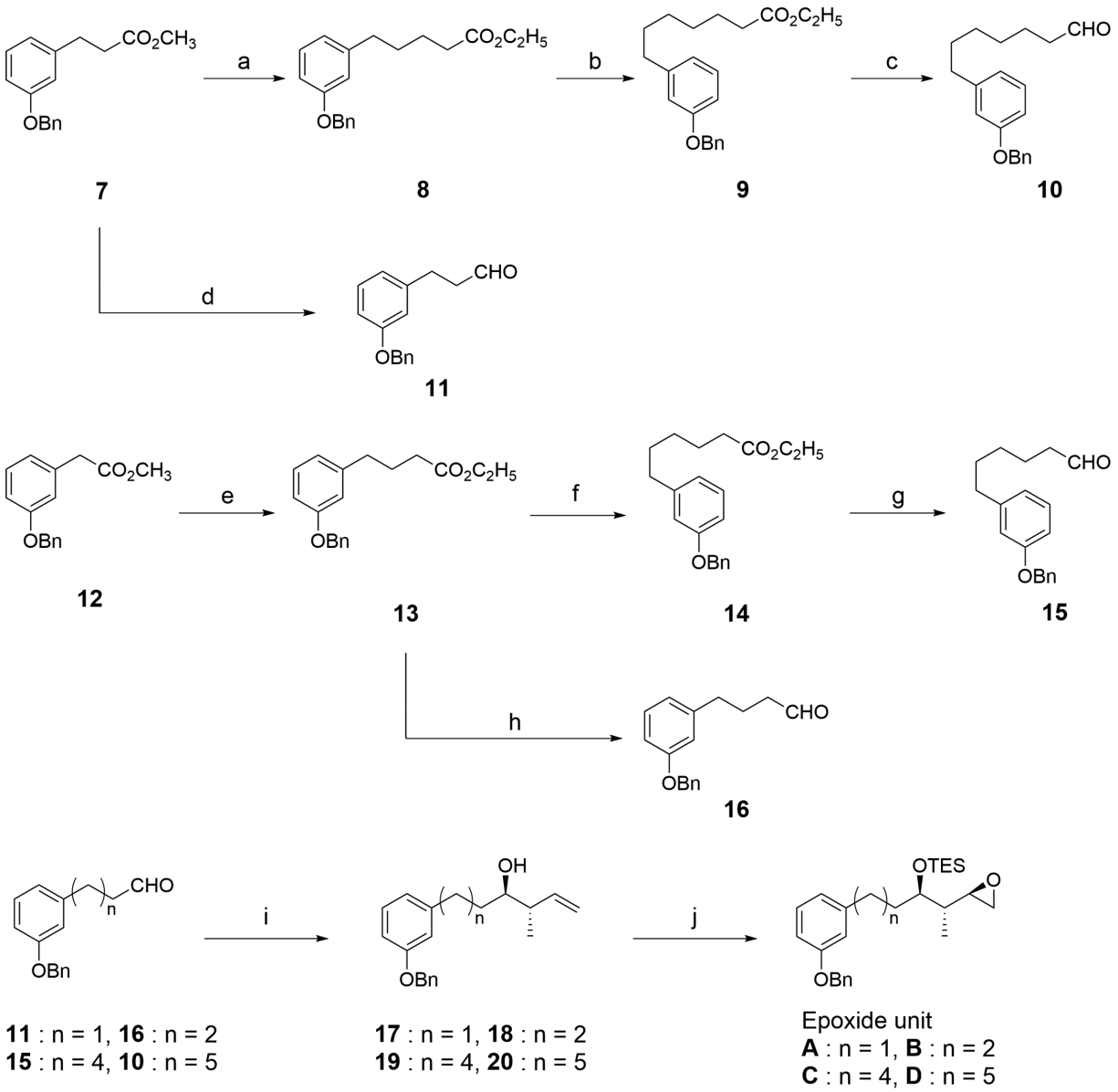

Scheme 2. Synthesis of the epoxide units **A**-**D**. (a) (1) $LiAlH_4$, THF, (2) CBr_4, PPh_3, DCM, 87% in two steps, (3) diethyl malonate, NaH, DMF, (4) LiCl, DMSO, H_2O, quant. in two steps; (b) (1) $LiAlH_4$, THF, 81%, (2) CBr_4, PPh_3, DCM, 98%, (3) diethyl malonate, NaH, DMF, 96%, (4) LiCl, DMSO, H_2O, 76%; (c) DIBAL-H, toluene, 97%; (d) DIBAL-H, toluene, 90%; (e) (1) $LiAlH_4$, THF, (2) CBr_4, PPh_3, DCM, 69% in two steps, (3) diethyl malonate, NaH, DMF, 81%, (4) LiCl, DMSO, H_2O, 64%; (f) (1) $LiAlH_4$, THF, quant., (2) CBr_4, PPh_3, DCM, 93%, (3) diethyl malonate, NaH, DMF, (4) LiCl, DMSO, H_2O, 48% in two steps; (g) DIBAL-H, toluene, 81%; (h) DIBAL-H, toluene, 87%; (i) *trans*-2-butene, *t*-BuOK, *n*-BuLi, (–)-Ipc_2BOMe, $n = 1$: 78%, $n = 2$: 72%, $n = 4$: 78%, $n = 5$: 84%; (j) (1) $VO(acac)_2$, TBHP, DCM, $n = 1$: 58%, $n = 2$: 44%, $n = 4$: 37%, $n = 5$: 47%, (2) TESCl, THF, $n = 1$: 87%, $n = 2$: 74%, $n = 4$: 77%, $n = 5$: 88%.

these peptides to the same extent as full-length of PKC isozymes (Shindo *et al.* 2001). The K_i values of **2-6** were calculated using the 50% inhibitory concentration (IC_{50}) obtained experimentally and the dissociation constants of each C1 peptide reported by Shindo *et al.* (2001) (Table 1).

The binding affinity of each derivative to PKCα-C1A and δ-C1B correlated well. The change of K_i values was dominated by that of the Clog *P* values: the higher the Clog *P* values, the smaller the K_i values. For example, introduction of a bromine atom into the phenol ring of **2** decreased the K_i value for PKCδ-C1B from 4.06 to 0.91 nM, which was comparable to that of **1** (0.54 nM). A similar change was observed in the K_i values for PKCα-C1A. However, none of these derivatives exhibited a higher binding potency than that of **1** against these PKC C1 peptides. Since the Clog *P* value of **1** (3.4) was less than that of **5** (4.5), these results indicate that the Clog *P* is not the only factor that dominates the binding ability to the PKC C1 peptides. In other words, the side chain length of **1** could affect not only hydrophobicity but also the spatial arrangement of the side chains and interactions with the PKC-C1 domains.

Antiproliferative activities of 2-6 against several cancer cell lines

Antiproliferative activities of **2-6** were evaluated by growth inhibition assay against 39 human cancer cell lines (Yamori *et al.* 1999). Growth inhibitory activity was expressed as GI_{50} (M), the

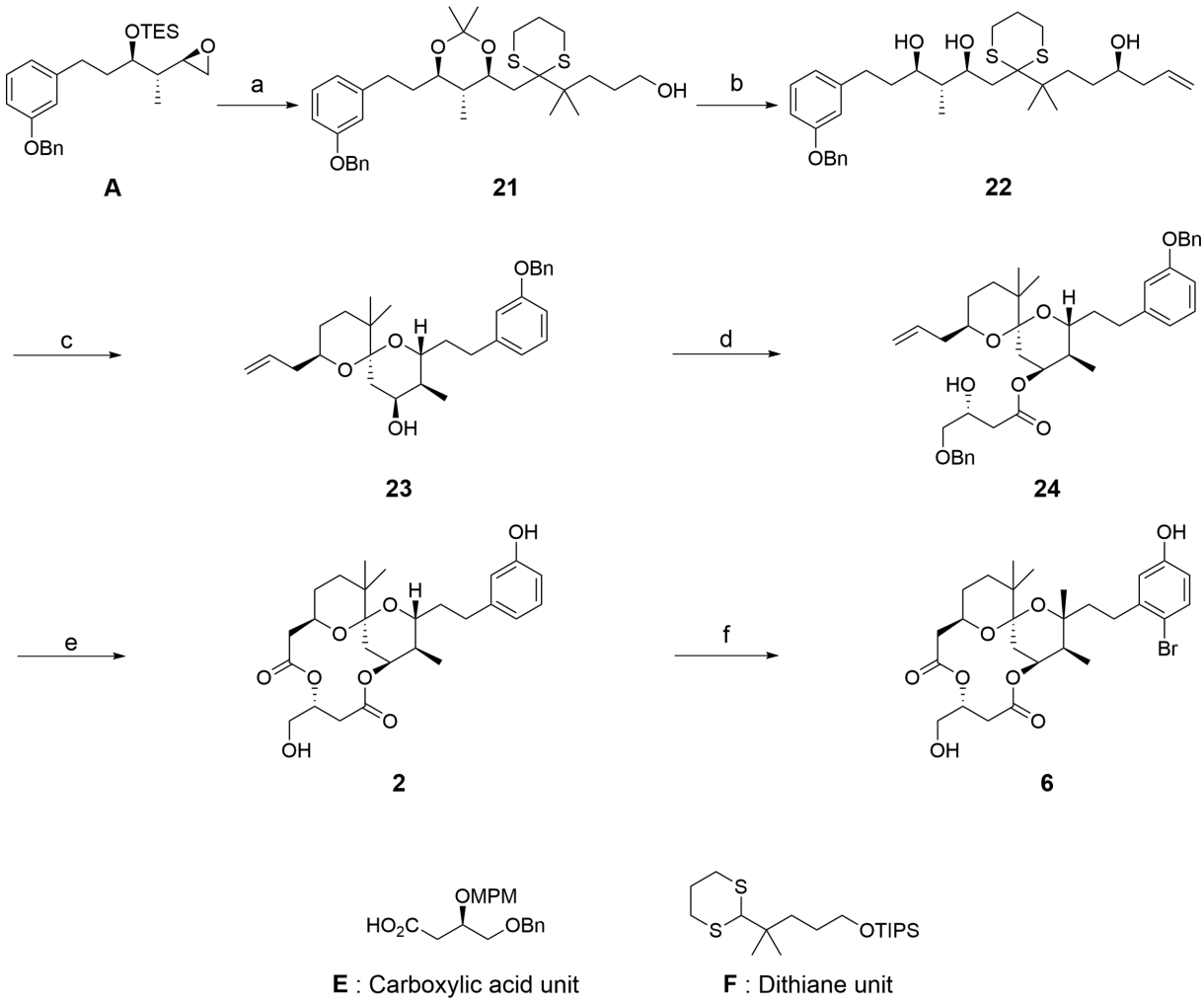

Scheme 3. Synthesis of **2** and **6**. (a) (1) **F**, *n*-BuLi in hexane, THF, quant., (2) $TsOH{\cdot}H_2O$, CH_3CN, THF, H_2O, 95%, (3) 2,2-dimethoxypropane, (+)-CSA, DCM, 87%; (b) (1) SO_3·Pyr, DMSO, Et_3N, DCM, 99%, (2) allyl-$SnBu_3$, $Ti(OiPr)_4$, $TiCl_4$, Ag_2O, (*S*)-BINOL, DCM, (3) $TsOH{\cdot}H_2O$, CH_3CN, THF, H_2O, 36% in two steps; (c) Selectfluor™, CH_3CN, H_2O, 42%; (d) (1) **E**, TCBCl, Et_3N, DMAP, (2) DDQ, pH 7.2 phosphate buffer, DCM, 85% in two steps; (e) (1) $KMnO_4$, $NaIO_4$, pH 7.2 phosphate buffer, 83%, (2) TCBCl, Et_3N, DMAP, toluene, 78%, (3) H_2, 10% Pd/C, EtOH, 96%; (f) $Bn(CH_3)_3NBr_3$, $CaCO_3$, DCM, MeOH, 54%.

Table 1. K_i values for the inhibition of [^{3}H]PDBu binding by **1-6** along with Clog *P* values

Compounds	1	2	3	4	5	6
Number of CH_2 (*n*)	4	2	3	5	6	2
Clog *P*	3.4	2.3	2.8	3.8	4.5	3.5
K_i (nM) for PKCα-C1A	6.03 (0.27)[a]	55.1 (9.6)	16.9 (1.6)	14.9 (0.2)	12.2 (1.3)	15.8 (1.1)
K_i (nM) for PKCδ-C1B	0.54 (0.01)	4.06 (0.42)	3.12 (0.22)	2.96 (0.20)	1.22 (0.06)	0.91 (0.19)

[a]Values in parenthesis are standard deviation.

concentration required to inhibit cell growth by 50% compared to an untreated control. Mean-graph midpoint value (MG-MID) was defined as the average log GI_{50} value for all 39 human cancer cell lines. Table 2 shows the log GI_{50} values for the 9 cancer cell lines whose log GI_{50} were less than an MG-MID value of **1**. The average log GI_{50} values of the 9 cancer cell lines are also listed. The rest of the data are provided in Supplemental Material.

The antiproliferative activities of **2** with the shortest side chain (n = 2) and **5** with the longest side chain (n = 6) were relatively weak compared to the others, while those of **3** (n = 3) and **4** (n = 5) were stronger than **2** and **5**, respectively. These results indicate that an optimal hydrophobicity for antiproliferative activities exists. In fact, **1** with a Clog *P* value of 3.4 exhibited the strongest anti-proliferative activity among the 6 derivatives in Table 2. However, the side chain length seems to also be important for the activities of **1**. The activity of the brominated **2** (**6**, n = 2) with a Clog *P* value of 3.5 was less than that of **1** (n = 4). Their PKC binding ability compared against that of PKCα-C1A and δ-C1B

Table 2. Growth inhibition [log GI_{50} (log M)] of **1-6** against aplog-sensitive human cancer cell lines

Cancer Type	Cell Line	1[a]	2	3	4	5	6	DAT[a]	TPA
Breast	HBC-4	−7.48	−6.37	−7.19	−6.67	−7.14	−7.15	−6.47	≤ −8
	MDA-MB-231	−6.90	−5.50	−5.91	−6.01	−6.09	−6.28	−6.03	−4.88
CNS	SNB-78	−6.05	−4.55	−4.73	−4.84	−4.77	−4.77	−4.80	−4.53
Colon	HCC2998	−6.47	−5.20	−6.14	−6.07	−5.51	−6.11	−6.08	≤ −8
Lung	NCI-H226	−6.15	−4.80	−4.84	−4.84	−4.88	−4.88	−4.93	−4.70
	NCI-H460	−7.07	−5.95	−6.68	−6.67	−6.79	−7.03	−6.46	≤ −8
	A549	−6.01	−5.50	−5.82	−5.52	−5.61	−6.46	−5.94	≤ −8
Melanoma	LOX-IMVI	−6.21	−4.90	−6.29	−5.82	−4.84	−5.47	−5.69	−4.70
Stomach	St-4	−6.24	−5.83	−6.93	−6.53	−5.43	−6.54	−6.44	≤ −8
Average		−6.51	−5.40	−6.06	−5.89	−5.67	−6.08	−5.87	≤−6.5
MG-MID		−5.24	−4.88	−5.20	−5.22	−5.08	−5.26	−5.22	≤−5.2

[a]Cited from reference Kikumori *et al.* 2012.

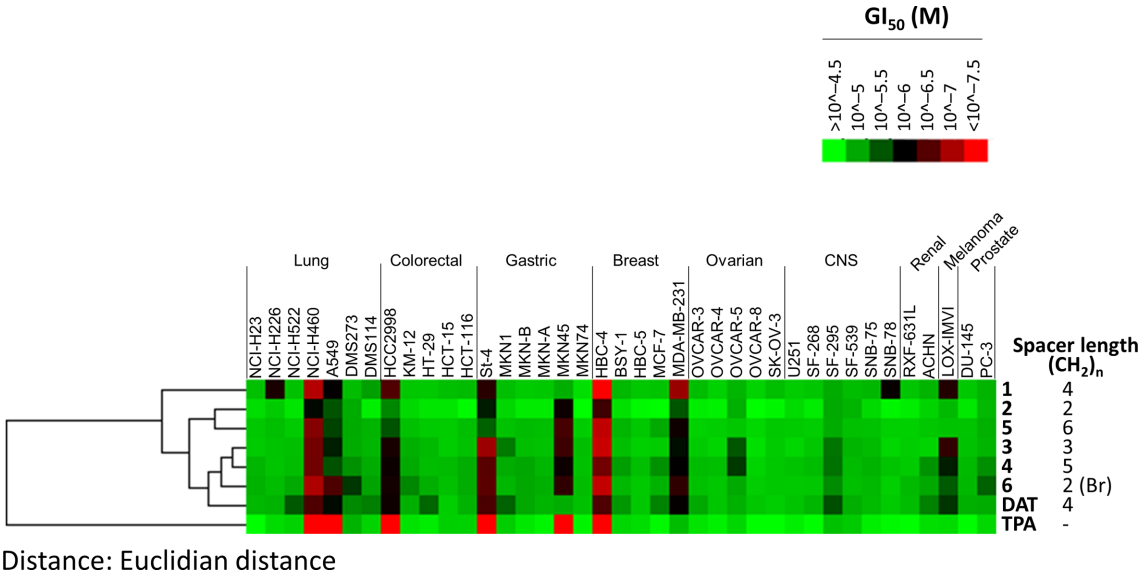

Figure 3. Efficacy profiles (fingerprints) of **1-6** along with DAT and TPA across the JFCR39 human cancer cell lines. The color of the heatmap represents GI_{50} concentrations (M) of each compound in each of the cell lines, as illustrated in the color bar; *i.e.* black represents 10^{-6} M (1 μM); red and green represent $10^{-7.5}$ M (31.6 nM) and $10^{-4.5}$ M (31.6 μM), respectively. Compounds were clustered on the basis of the similarity with other compounds (average-linkage clustered with Euclidian distance). Cluster analysis and visualization by heatmap was performed by using Cluster3.0/TreeView software (Stanford University).

(Table 1) correlated generally with their anti-proliferative activity.

Figure 3 shows heatmap (fingerprints) and hierarchical cluster analysis for log GI_{50} values of **1-6** along with those of DAT and TPA against 39 human cancer cell lines. The above mentioned 9 cell lines exhibited sensitivity to these PKC ligands, especially to **1**. The fingerprints of **1-6**, DAT and TPA exhibit significant correlation (Pearson's correlation coefficient > 0.7, except for **1** versus TPA) each other as shown in Table 3, suggesting their similar mode of action in the antiproliferative activities. Since all these compounds are PKC ligands, their main targets could be PKC isozymes as mentioned above (Hanaki *et al.* 2018).

Table 3. Pearson correlation coefficients between log GI_{50} fingerprints of **1-6** along with DAT and TPA

Compounds	1	2	3	4	5	6	DAT	TPA
1	1	0.75	0.81	0.81	0.77	0.81	0.82	0.68
2	0.75	1	0.92	0.92	0.93	0.95	0.78	0.89
3	0.81	0.92	1	0.97	0.85	0.92	0.86	0.86
4	0.81	0.92	0.97	1	0.87	0.93	0.86	0.85
5	0.77	0.93	0.85	0.87	1	0.92	0.74	0.82
6	0.81	0.95	0.92	0.93	0.92	1	0.87	0.90
DAT	0.82	0.78	0.86	0.86	0.74	0.87	1	0.77
TPA	0.68	0.89	0.86	0.85	0.82	0.90	0.77	1

Proinflammatory activities of 2-6 on mouse ear

Since the hydrophobicity of the molecule was closely related to the adverse effects of the PKC ligands, proinflammatory and tumor-promoting activity (Szállási *et al.* 1993; Kishi and Rando 1998), and since these adverse effects correlated well with each other (Philip *et al.* 2004), the proinflammatory activities of **2-6** along with **1** were evaluated by the mouse ear edema test. The effect of the introduction of a bromine atom was examined in **6**. Each compound in various doses (1.7, 17, and 170 nmol) was applied to 1 ear of each ICR (Institute of Cancer Research) mouse

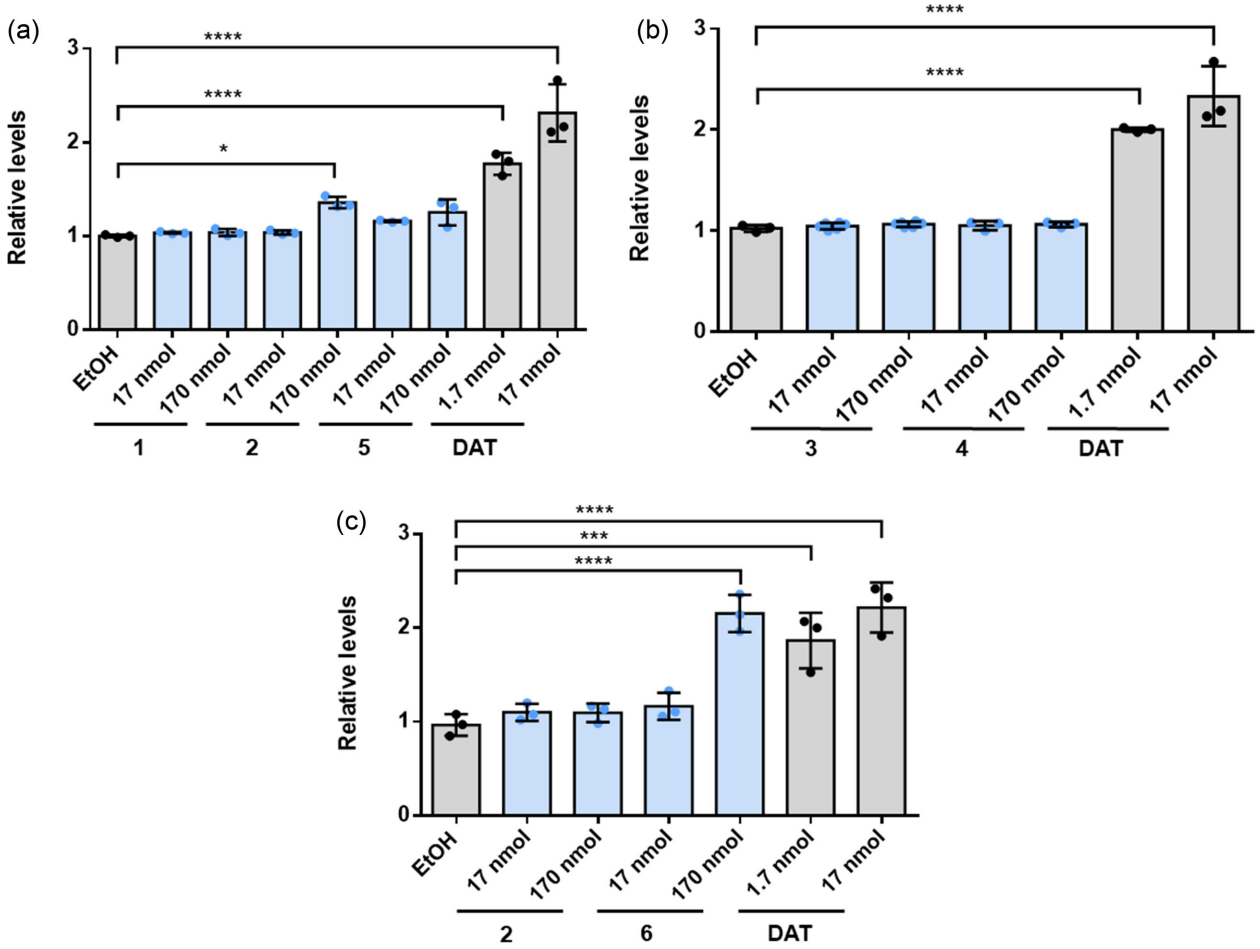

Figure 4. Change in the relative weight of the mouse ear 24 h after the application of **1-6** and DAT. (a) **1**, **2**, **5**, and DAT; (b) **3**, **4**, and DAT; (c) **2**, **6**, and DAT. Error bars show the standard deviation of 3 samples. $^{*}P < .05$ versus vehicle (EtOH) alone; $^{**}P < .01$; $^{***}P < .001$; and $^{****}P < .0001$ (Dunnett's test).

and the weight of the ear was measured after 24 h as reported previously (Kikumori *et al.* 2016). The value relative to the weight of the untreated ear (EtOH only) was used as an index of the proinflammatory activity. As shown in Figure 4a and b, DAT induced significant inflammation even at 1.7 nmol, whereas compounds **1-5** without a bromine atom at the phenol ring exhibited little or no proinflammatory activity even when applied at 170 nmol. On the other hand, **6**, a brominated derivative of **2**, exhibited significant proinflammatory activity at 170 nmol (Figure 4c). These results suggest that the introduction of a bromine atom to the phenol ring of aplogs to increase their hydrophobicity is not suitable for developing a new PKC ligand with therapeutic potential. This result is consistent with the fact that ATX with a bromine atom is more proinflammatory than DAT (Shimomura *et al.* 1983; Suganuma *et al.* 1984). A similar tendency was observed in **1** and its brominated analog as reported previously (Kikumori *et al.* 2016).

Molecular modeling study of PKCδ-C1B domain in complex with 1-5

Despite 10-methyl-aplog-1 (**1**) having an intermediate molecular hydrophobicity (Clog $P = 3.4$) among the evaluated compounds (Clog $P = 2.3$-4.5), it had the highest affinity for PKCδ-C1B domain ($K_i = 0.54$ nM), as shown in Table 1. Since the optimal log P of aplog-1 for antiproliferative activities against several cancer cell lines was 4.0-4.5 (Kamachi *et al.* 2013), **1** has a relatively high affinity for PKC C1 domains considering its log P (3.3) (Kamachi *et al.* 2013). To gain insights into its relatively high affinity, we performed molecular dynamics (MD) simulation of the membrane-embedded PKCδ-C1B domain in complex with **1-5**, followed by the Molecular Mechanics Poisson–Boltzmann Surface Area (MM-PBSA) calculation of the end-point binding free energy. Because the MM-PBSA calculation provides a binding free energy in aqueous solution ($\Delta E_{\text{MM-PBSA}}$), the binding free energies in the presence of phospholipids ($\Delta G^{\circ}_{\text{bind}}$) were calculated as a sum of $\Delta E_{\text{MM-PBSA}}$ and $\Delta G^{\circ}_{\text{transfer}}$ which is the cytosol-to-membrane transfer free energy of the protein/ligand complex calculated by the PPM server based on the Orientations of Proteins in Membrane (OPM) database (Lomize *et al.* 2012).

The initial structures of the PKCδ-C1B domain/phorbol 13-acetate complex (PDB code: 1PTR) were created by the AutoDock-GPU program (version 4.2.6) (Morris *et al.* 2009). Those structures were embedded in a 1-palmitoyl-2-oleoylphosphatidylserine (POPS) bilayer membrane by the PPM server and the CHARMM-GUI server (Jo *et al.* 2008; Lee *et al.* 2016). The MD simulations were performed by the GROMACS program (version 2020.2) (Van der Spoel *et al.* 2005). According to the ESMACS (enhanced sampling of molecular dynamics with an approximation of continuum solvent) protocol proposed by Wan *et al.* (2015), 25 replicas of the membrane/protein/ligand complex in explicit water were subjected to the equilibration steps with

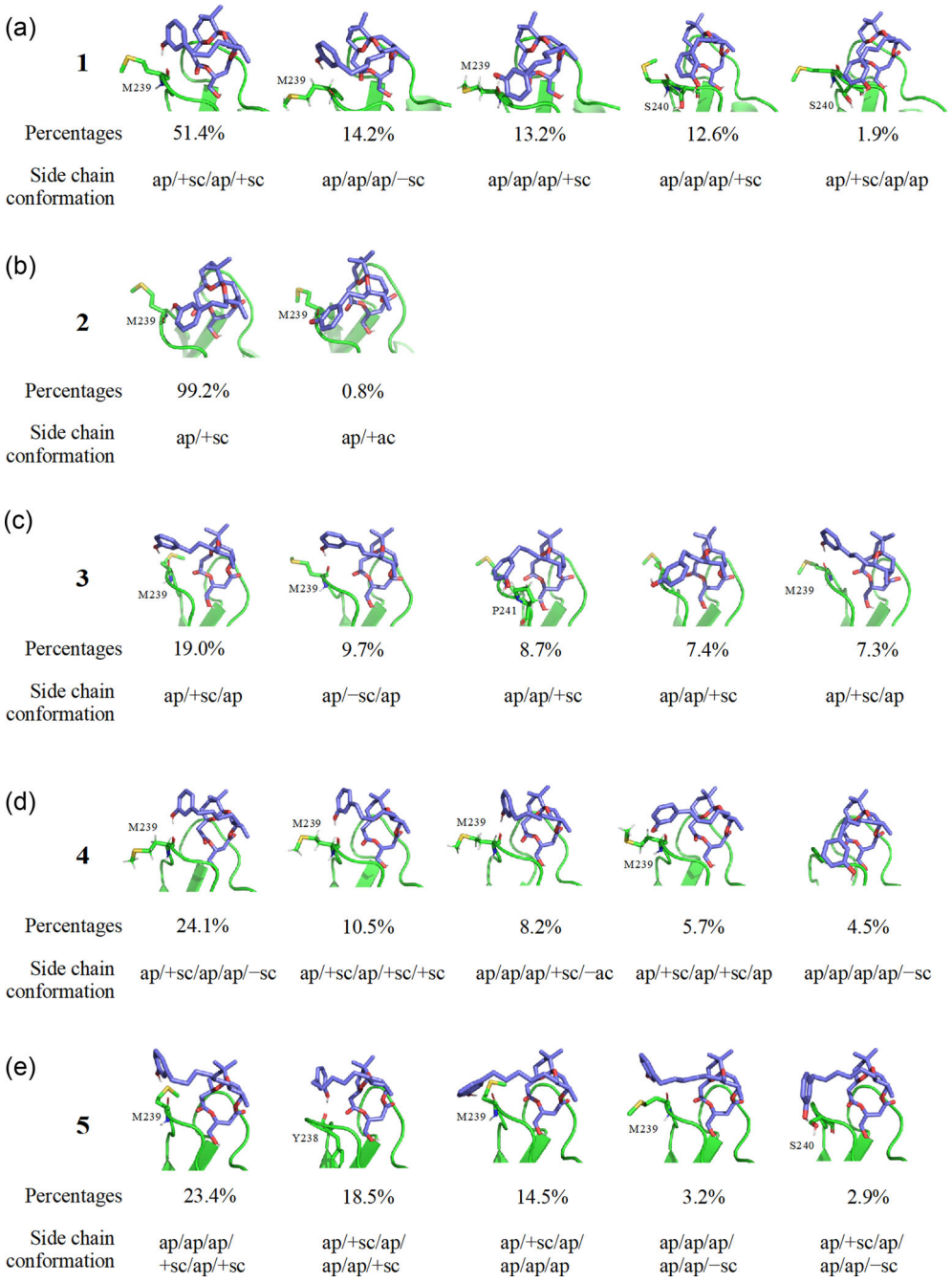

Figure 5. Top 5 conformers of **1-5** (**a-e**) in the bound state during MD simulation. ap, +sc, –sc, +ac, and –ac indicate antiperiplanar (± 150° to 180°), +synclinal (30° to 90°), –synclinal (−30° to −90°), +anticlinal (90° to 150°), and –anticlinal (−90° to −150°) conformations, respectively. Nonpolar hydrogen atoms are not shown.

position and dihedral angle restraints and 2 ns of MD run without any restraints. Then, 4 ns of production MD runs were executed (snapshots for every 100 ps). The 4 ns trajectories from the 25 replicas were aggregated to produce a 100 ns trajectory, which was subjected to the MM-PBSA calculation using the MMPBSA.py script (Miller *et al.* 2012) in the AmberTools 19 package (Case *et al.* 2019). In order to cancel out noisy bonded terms, the single trajectory approach for the MM-PBSA analysis was employed. The final coordinate of the protein/ligand complex in each replica was analyzed by the PPM server to estimate $\Delta G^{\circ}_{transfer}$.

The docking simulation gave docked structures of **2-4** where their phenolic hydroxy groups formed hydrogen bonding with the carbonyl group of Met-239 of the PKCδ-C1B domain as previously predicted for **1** (Figure 5b-d) (Hanaki *et al.* 2017). The phenolic hydroxy group in **5** formed hydrogen bonding with the carbonyl groups of Tyr-238 and Met-239, and the side chain of Ser-240 (Figure 5e). Although these predictions were supported by the MD simulation, this also suggested that the side chain conformations of the ligands are highly variable in the bound states (Figure 5).

Table 4. $\Delta E_{MM\text{-}PBSA}$ and $\Delta G^{o}_{transfer}$ values for **1-5**

Compd.	$\Delta E_{MM\text{-}PBSA}$ (A)	$\Delta G^{o}_{transfer}$[b] (B)	Predicted ΔG^{o}_{bind} (A + B)	Experimental ΔG^{o}_{bind}[c]	
1	−8.4441 (1.0063)[a]	−10.9 (0.2)	−19.3 (1.6)	−13.13	(kcal mol^{-1})
2	−9.0920 (0.9882)	−10.6 (0.2)	−19.7 (1.6)	−11.71	(kcal mol^{-1})
3	−9.2323 (1.0159)	−9.7 (0.2)	−18.9 (1.7)	−12.11	(kcal mol^{-1})
4	−8.0480 (0.9826)	−11.4 (0.2)	−19.4 (1.5)	−12.06	(kcal mol^{-1})
5	−8.0120 (1.0136)	−12.6 (0.2)	−20.6 (1.5)	−12.48	(kcal mol^{-1})

[a]Standard error of the mean: $n = 1000$ for A, and $n = 25$ for B.
[b]Calculated by the PPM server (Lomize *et al.* 2012).
[c]Experimental $\Delta G^{o}_{bind} = (1/4184) \times -RT \ln (C^{o} K_i^{-1})$, where R is the gas constant (8.31446 J/K/mol), $T = 310$ (K), and C^{o} is the standard concentration (1 M).

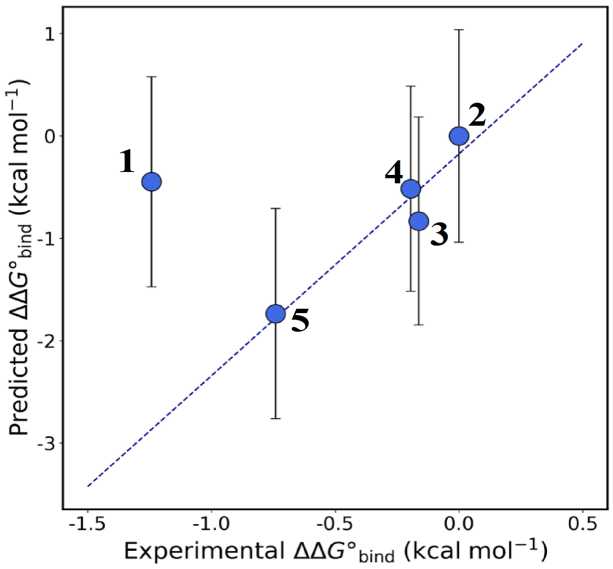

Figure 6. Correlation between experimental and predicted relative binding free energy ($\Delta\Delta G^{o}_{bind}$) of **1-5**. Error bars indicate standard error of the means (SEM). The dashed line is a least-squares regression line for **2-5**.

Table 4 lists the predicted ΔG^{o}_{bind} (the sum of $\Delta E_{MM\text{-}PBSA}$ and $\Delta G^{o}_{transfer}$) and the experimental ΔG^{o}_{bind} of the ligands. As depicted in Figure 6, there was a strong positive correlation (Pearson's $r = 0.958$) between the predicted and the experimental $\Delta\Delta G^{o}_{bind}$ for **2-5**. However, the predicted affinity of **1** ($\Delta G^{o}_{bind} = -19.3$ kcal mol^{-1}) was almost the same as that of **4** ($\Delta G^{o}_{bind} = -19.4$ kcal mol^{-1}); experimentally, the affinity of **1** was approximately 6 times higher than that of **4**. Because the single trajectory approach for the MM-PBSA calculation (Gilson and Zhou 2007) did not account for changes in potential energy of both the receptor and the ligands in the binding process and did not also include entropy change, the relatively high affinity of **1** could be attributed to those factors.

In terms of conformational distribution in the bound state, it is noteworthy that the main conformer of **1** in the bound state (Figure 5a, leftmost) accounted for 51.4%, which was substantially larger than the other ligands except for **2**, which has the smallest conformational space. It appears that the main conformer of **1** is stabilized by intramolecular CH/π interactions between the methyl group at position 6 and the aromatic ring. This conjecture was supported by comparison of the potential energies of the ligands in the bound state and the aqueous solution by the MD simulation. Table 5 lists the change of potential energy of the ligands in the binding process (ΔU^{o}_{ligand}) and their van der Waals energy components. The potential energy of **1** was significantly lowered in the binding process ($\Delta U^{o}_{ligand} = -4.94$ kcal/mol), which was attributed to the lowering of the van der Waals energy components. Note that the ΔU^{o}_{ligand} of **4** was larger than that of **1**. The binding of **4** might be hindered by entropic factors as its bond in the side chain rotates more easily and should, therefore, lose a larger amount of conformational entropy upon binding (O'Boyle *et al.* 2011).

Conclusions

In this study, a series of side chain derivatives of 10-methyl-aplog-1 (**1**) were synthesized and their biological activities were evaluated to optimize the side chain length of **1** as a promising therapeutic agent for cancer. The PKC binding affinities of **2-5** were lower than that of **1** (Table 1), and the antiproliferative activities against several cancer cell lines generally correlated with the binding ability to the PKCα-C1A and δ-C1B domains that are involved in antiproliferative activities (Hanaki *et al.* 2018). Although the hydrophobicity of the molecule played a critical role in the PKC binding and antiproliferative activities, the introduction of a bromine atom to the phenol moiety of **2** increased proinflammatory activity as well as these activities. These data clearly indicate that **1** has an optimal side chain length to show antiproliferative activity with little adverse effects, and that the introduction of a bromine atom into the

Table 5. Difference between average total potential energies in the bound and unbound states (ΔU^{o}_{ligand}) for **1-5**

Compounds	ΔU^{o}_{ligand}	Components		vdW Energy	
		LJ-14[a] (A)	LJ (SR)[b] (B)	(A + B)	
1	−4.94	1.48	−6.58	−5.09	(kcal mol^{-1})
2	−1.86	0.06	−4.23	−4.17	(kcal mol^{-1})
3	4.31	1.73	−0.53	1.20	(kcal mol^{-1})
4	−7.55	1.77	−9.05	−7.28	(kcal mol^{-1})
5	−3.88	1.46	−2.65	−1.19	(kcal mol^{-1})

[a]Intramolecular Lennard–Jones potential energy between i and $i + 3$ atoms (1-4 interactions).
[b]Intramolecular short-range (i.e., within the nonbonded cutoff) Lennard–Jones potential energy between i and $i + n$ ($n > 3$) atoms.

phenol ring in the side chain to increase the hydrophobicity is not a suitable method for designing new anticancer drug seeds. Finally, the molecular modeling study suggested that the relatively high affinity of **1** may come from: (1) a larger intramolecular van der Waals interaction that stabilizes the conformation in the bound state; and (2) a smaller loss of conformational entropy upon binding that can be effectively compensated by the above interactions.

Experimental section

General remarks

The following spectroscopic and analytical instruments were used: ^{1}H and ^{13}C NMR, AVANCE III 400 and AVANCE III 500 (ref. TMS, Bruker, Germany); HPLC, model 600E with a model 2487 UV detector (Waters, Tokyo, Japan); HR-FAB-MS and JMS-MS700V (JEOL, Tokyo, Japan); timsTOF (Bruker, Germany); HR-ESI-TOF-MS, Xevo G2-S-qTOF (Waters, Tokyo, Japan); FT/IR, FT/IR-470 Plus (Jasco, Tokyo, Japan); and digital polarimeter, P2200 (Jasco, Tokyo, Japan). HPLC was carried out on a YMC-packed ODS-A AA12S05-1520WT, SIL SL12S05-2510WT (YMC, Kyoto, Japan), and CHIRALCEL OJ-RH (Daicel Corporation, Osaka, Japan). Wakogel C-200 (silica gel, FUJI FILM Wako Pure Chemical Corporation, Osaka, Japan) and YMC*GEL ODS-A S-50 μm 12 nm (YMC, Kyoto, Japan) were used for column chromatography. [^{3}H]PDBu (18.7 Ci/mmol) was obtained from PerkinElmer Life Sciences Research Products (Boston, MA, USA) by custom synthesis. The PKC C1 peptides were synthesized as reported previously (Shindo *et al.* 2001). All other reagents were purchased from chemical companies and used without further purification. ICR mice were purchased from Shimizu Laboratory Supplies (Kyoto, Japan). Animal experiments were approved by the Animal Care Committee of Kyoto University and implemented according to the regulations.

Inhibition of specific binding of [^{3}H]PDBu to PKC C1 peptides

The binding of [^{3}H]PDBu to the PKCδ-C1B peptides was evaluated by the procedure of Sharkey and Blumberg (Sharkey and Blumberg 1985), with modifications as reported previously (Shindo *et al.* 2001), using 50 mM Tris-maleate buffer (pH 7.4 at 4 °C), 13.8 nM PKCδ-C1B peptides, 20 nM [^{3}H]PDBu (18.7 Ci/mmol), 50 μg/mL 1,2-dioleoyl-*sn*-glycero-3-phospho-L-serine (Sigma–Aldrich), 3 mg/mL bovine γ-globulin (Sigma–Aldrich), and various concentrations of inhibitors. In the PKCα-C1A binding assay, a peptide concentration of 20 nM was employed. Binding affinity was evaluated based on the concentration required to cause 50% inhibition of the specific binding of [^{3}H]PDBu (IC_{50}) which was calculated by a computer program with a log-probit procedure. The inhibition constant (K_i) was calculated by the method of Sharkey and Blumberg (Sharkey and Blumberg 1985).

Measurements of cell growth inhibition

A panel of 39 human cancer cell lines established by Yamori and colleagues according to the National Cancer Institute (NCI) method with modifications was employed, and cell growth inhibitory activity was measured as reported previously (Yamori *et al.* 1999). In brief, the cells were plated in 96-well plates on a RPMI 1640 medium supplemented with 5% fetal bovine serum and allowed to attach overnight. The cells were incubated with each test compound for 48 h, and cell growth was estimated by the sulforhodamine B assay. The 50% growth inhibition (GI_{50}) parameter was calculated as reported previously (Yamori *et al.* 1999). Absorbance for the control well (C) and the test well (T) was measured at 525 nm along with that for the test well at time 0 (T_0). Cell growth inhibition (% growth) by each concentration of drug (10^{-8}, 10^{-7}, 10^{-6}, 10^{-5}, and 10^{-4} M) was calculated as $100[(T-T_0)/(C-T_0)]$ using the average of duplicate points. By processing of these values, each GI_{50} value, defined as $100\ [(T-T_0)/(C-T_0)] = 50$, was determined.

Mouse ear edema test

This test was performed by the method reported previously (Kikumori *et al.* 2016; Hanaki *et al.* 2017). In brief, 17 nmol or 170 nmol of each test compound in EtOH (10 µL), and 1.7 nmol and 17 nmol of DAT in EtOH (10 µL), was applied to the right ear of 5-week-old ICRs, and EtOH (10 µL) was applied to the left ear by means of a micropipette. After 24 h, a disk (0.8 cm square) was obtained from the ear and weighed. Each group consisted of at least 3 mice. Statistical analysis was performed using the scientific data analysis software GraphPad Prism version 6 (GraphPad Software) with 1-way analysis of variance followed by Dunnett's test. Statistical significance is indicated in figure legends as $^{*}P < .05$ versus vehicle alone; $^{**}P < .01$; $^{***}P < .001$; and $^{****}P < .0001$.

Molecular modeling study

Docking simulation: The crystal structure of the PKCδ-C1B domain/phorbol 13-acetate complex (PDB code: 1PTR) was obtained from the Protein Data Bank. The Gasteiger-Marsili sigma partial charges were assigned to the ligands using the Open Babel program (O'Boyle *et al.* 2011). The docking experiment was performed with AutoDock-GPU (version 4.2.6) and MGLTools 1.5.7 RC1. Lamarckian Genetic Algorithm was employed as the docking algorithm. A docking grid was set around the ligand-binding cleft of the receptor. Docking parameters were: number of Genetic Algorithm (GA) runs, 200; population size, 150; maximum number of evaluation, 25 000 000; maximum number of generations, 27 000.

MD simulation: Missing side-chains (Lys-234, Arg-274, and Glu-274) were automatically added to the crystal structure of the PKCδ-C1B domain using the Swiss PDB Viewer (Guex and Peitsch 1997). Glycine residues were added to the N- and C-termini. An initial model of the POPS–ligand–PKCδ-C1B ternary complex in a rectangular box filled by TIP3P water was constructed using the CHARMM-GUI Bilayer Builder (Jo *et al.* 2008; Lee *et al.* 2016) and the PPM Server (Lomize *et al.* 2012) as reproducing the membrane binding model of the C1 domain calculated by Lomize *et al.* (2012). *Z*-length of the simulation box was determined by water thickness (minimum water height on top and bottom of the system was set to 22.5 Å), and initial XY-lengths were set to 62 Å. The net charge on the system was neutralized by adding 150 mM of KCl. The numbers of lipid molecules in the upper and lower leaflets were 64 and 58, respectively. The AMBER ff14SB force field, the Zinc AMBER Force Field (ZAFF) (Peters *et al.* 2010), and GAFF2 force field were used to describe the system. Coordination of cysteine and histidine residues to zinc ions was treated as single bonds with tetrahedral geometry.

All MD simulations were performed using the GROMACS program (version 2020.2). The geometry for the system was a rectangular box with periodic boundary conditions. The system was gradually relaxed according to CHARMM-GUI-generated

position and angle restraint conditions to reach equilibrium (310 K, 1 bar). Then, 2 ns NPT (constant number of atoms, pressure, and temperature) simulation without any position restraints with a 2 fs time-step was performed. Production NPT simulations were performed for 4 ns with a 2 fs time-step. This production run was repeated 25 times to produce 100 ns of trajectory for each ligand. In the NPT simulation, temperature and pressure were regulated using the V-rescale thermostat algorithm and the Parinello–Rahman barostat algorithm, respectively. The time constant for the temperature and pressure coupling was kept at 0.5 and 5 ps, respectively. The pressure was coupled with a semi-isotropic scheme with isothermal compressibility of 4.5×10^{-5} bar^{-1}. The short-range nonbonded interactions were computed for the atom pairs within the cutoff of 1.2 nm, while the long-range electrostatic interactions were calculated using a particle-mesh-Ewald summation method with fourth-order cubic interpolation and 0.16 nm grid spacing. All bonds were constrained using the parallel LINCS method. The center of mass translations of the membrane, ligand/protein, and water/ion were removed at an interval of every 100 time-steps.

MM/PBSA calculation was performed by the MMPBSA.py.MPI (Miller *et al*. 2012) module in AmberTools 19 (Case *et al*. 2019), External and internal dielectric constants were set to 80 and 1, respectively. Ion strength was set to 0.200.

The final coordinate of the protein/ligand complex in each replica was analyzed by the PPM server (Lomize *et al*. 2012) to estimate $\Delta G^{\circ}_{transfer}$.

Acknowledgments

The authors thank the Molecular Profiling Committee, Grant-in-Aid for Scientific Research on Innovative Areas "Advanced Animal Model Support (AdAMS)" from the Ministry of Education, Culture, Sports, Science and Technology, Japan (JSPS KAKENHI Grant Number JP 16H06276). They also thank Ms. Akiko Fujihashi in the Joint Usage/Research Center (JURC) at the Institute for Chemical Research, Kyoto University, Japan, for mass measurements with the JEOL JMS-MS700V spectrometer and the Bruker timsTOF instrument.

Supplementary material

Supplementary material is available at *Bioscience, Biotechnology, and Biochemistry* online. Synthesis of 2-6 and their spectral data, along with those of their synthetic intermediates, and their efficacy profiles (fingerprints) against 39 human cancer cell lines are included in the Supplemental Material available at http://dx.doi.org/xxx.

Author contribution

K.I. designed the study. A.G. and K.T. synthesized compounds **2-6** and evaluated their biological activities. S.D. measured the antiproliferative activities of **2-6** using the panel of 39 cancer cell lines. R.C.Y. carried out the computational studies. K.I., A.G., and R.C.Y. wrote the manuscript.

Funding

This work was supported by JSPS KAKENHI [Grant Number 17H06405] to K.I. and R.C.Y.

Disclosure statement

The authors reported no conflicts of interest.

References

Andersen RJ, Ntie-Kang F, Tietjen I. Natural product-derived compounds in HIV suppression, remission, and eradication strategies. *Antiviral Res* 2018;**158**:63-77.

Antal CE, Hudson AM, Kang E *et al*. Cancer-associated protein kinase C mutations reveal kinase's role as tumor suppressor. *Cell* 2015;**160**:489-502.

Antal CE, Newton AC. Tuning the signaling output of protein kinase C. *Biochem Soc Trans* 2014;**42**:1477-83.

Bignami GS, Wagner F, Grothaus PG *et al*. Biological activity of 26-succinylbryostatin 1. *Biochim Biophys Acta* 1996;**1312**:197-206.

Brown HC, Bhat KS. Enantiomeric (*Z*)- and (*E*)-crotyldiisopinocampheylboranes. Synthesis in high optical purity of all four possible stereoisomers of β-methylhomoallyl alcohols. *J Am Chem Soc* 1986;**108**:293-4.

Case DA, Ben-Shalom IY, Brozell SR *et al*. *AMBER 2019*, University of California, San Francisco.

Fujiki H, Sugimura T. New classes of tumor promoters: teleocidin, aplysiatoxin, and palytoxin. *Adv Cancer Res* 1987;**49**:223-64.

Fujiki H, Tanaka Y, Miyake R *et al*. Activation of calcium-activated, phospholipid-dependent protein kinase (protein kinase C) by new classes of tumor promoters: teleocidin and debromoaplysiatoxin. *Biochem Biophys Res Commun* 1984;**120**:339-43.

Gilson MK, Zhou HX. Calculation of protein-ligand binding affinities. *Annu Rev Biophys Biomol Struct* 2007;**36**:21-42.

Guex N, Peitsch MC. SWISS-MODEL and the Swiss-PdbViewer: An environment for comparative protein modeling. *Electrophoresis* 1997;**18**:2714-23.

Gutiérrez C, Serrano-Villar S, Madrid-Elena N *et al*. Bryostatin-1 for latent virus reactivation in HIV-infected patients on antiretroviral therapy. *AIDS* 2016;**30**:1385-92.

Hanaki Y, Kikumori M, Tokuda H *et al*. Loss of the phenolic hydroxyl group and aromaticity from the side chain of antiproliferative 10-methyl-aplog-1, a simplified analog of aplysiatoxin, enhances its tumor-promoting and proinflammatory activities. *Molecules* 2017;**22**:631.

Hanaki Y, Shikata Y, Kikumori M *et al*. Identification of protein kinase C isozymes involved in the anti-proliferative and pro-apoptotic activities of 10-methyl-aplog-1, a simplified analog of debromoaplysiatoxin, in several cancer cell lines. *Biochem Biophys Res Commun* 2018;**495**:438-45.

Hanawa H, Uraguchi D, Konishi S *et al*. Catalytic asymmetric allylation of aldehydes and related reactions with bis (((*S*)-binaphtoxy) (isopropoxy)titanium) oxide as a μ-oxo-type chiral lewis acid. *Chem Eur J* 2003;**9**:4405-13.

Inanaga J, Hirata K, Saeki H *et al*. A rapid esterification by means of mixed anhydride and its application to large-ring lactonization. *Bull Chem Soc Jpn* 1979;**52**:1989-93.

Irie K, Kikumori M, Kamachi H *et al*. Synthesis and structure–activity studies of simplified analogues of aplysiatoxin with antiproliferative activity like bryostatin-1. *Pure Appl Chem* 2012;**84**:1341-51.

Irie K, Oie K, Nakahara A *et al*. Molecular basis for protein kinase C isozyme-selective binding: The synthesis, folding, and phorbol ester binding of the cysteine-rich domains of all protein kinase C isozymes. *J Am Chem Soc* 1998;**120**:9159-67.

Isakov N. Protein kinase C (PKC) isoforms in cancer, tumor promotion and tumor suppression. *Semin Cancer Biol* 2018;**48**: 36-52.

Jo S, Kim T, Iyer VG *et al*. CHARMM-GUI: A web-based graphical user interface for CHARMM. *J Comput Chem* 2008;**29**:1859-65.

Kajigaeshi S, Kakinami T, Tokiyama H *et al*. Bromination of phenols by use of benzyltrimethylammonium tribromide. *Chem Lett* 1987;**16**:627-30.16

Kamachi H, Tanaka K, Yanagita RC *et al*. Structure–activity studies on the side chain of a simplified analog of aplysiatoxin (aplog-1) with anti-proliferative activity. *Bioorg Med Chem* 2013;**21**:2695-702.

Kato Y, Scheuer PJ. Aplysiatoxin and debromoaplysiatoxin, constituents of the marine mollusk *Stylocheilus longicauda*. *J Am Chem Soc* 1974;**96**:2245-6.

Kikumori M, Yanagita RC, Tokuda H *et al*. Structure–activity studies on the spiroketal moiety of a simplified analogue of debromoaplysiatoxin with antiproliferative activity. *J Med Chem* 2012;**55**:5614-26.

Kikumori M, Yanagita RC, Tokuda H *et al*. Structural optimization of 10-methyl-aplog-1, a simplified analog of debromoaplysiatoxin, as an anticancer lead. *Biosci Biotechnol Biochem* 2016;**80**:221-31.

Kishi Y, Rando RR. Structural basis of protein kinase C activation by tumor promoters. *Acc Chem Res* 1998;**31**:163-72.

Kollár P, Rajchard J, Balounová Z *et al*. Marine natural products: bryostatins in preclinical and clinical studies. *Pharm Biol* 2014;**52**:237-42.

Lee J, Cheng X, Swails JM *et al*. CHARMM-GUI Input Generator for NAMD, GROMACS, AMBER, OpenMM, and CHARMM/OpenMM Simulations using the CHARMM36 Additive Force Field. *J Chem Theory Comput* 2016;**12**:405-13.

Liu J, Wong CH. An efficient method for the cleavage of *p*-methoxybenzylidene (PMP), tetrahydropyranyl (THP) and 1,3-dithiane protecting groups by Selectfluor™. *Tetrahedron Lett* 2002;**43**:4037-9.

Lomize MA, Pogozheva ID, Joo H *et al*. OPM database and PPM web server: resources for positioning of proteins in membranes. *Nucleic Acids Res* 2012;**40**: D370-376.

Miller BR, III, McGee TD, Jr, Swails JM *et al*. MMPBSA.py: An efficient program for end-state free energy calculations. *J Chem Theory Comput* 2012;**8**:3314-21.

Morris GM, Huey R, Lindstrom W *et al*. Autodock4 and AutoDockTools4: automated docking with selective receptor flexibility. *J Comput Chem* 2009;**30**:2785-91.

Mutter R, Wills M. Chemistry and clinical biology of the bryostatins. *Bioorg Med Chem* 2000;**8**:1841-60.

Nakagawa Y, Yanagita RC, Hamada N *et al*. A simple analogue of tumor-promoting aplysiatoxin is an antineoplastic agent rather than a tumor promoter: development of a synthetically accessible protein kinase C activator with bryostatin-like activity. *J Am Chem Soc* 2009;**131**:7573-9.

Nelson TJ, Alkon DL. Neuroprotective versus tumorigenic protein kinase C activators. *Trends Biochem Sci* 2009;**34**: 136-45.

Nishizuka Y. Studies and perspectives of protein kinase C. *Science* 1986;**233**:305-12.

Nishizuka Y. Intracellular signaling by hydrolysis of phospholipids and activation of protein kinase C. *Science* 1992;**258**:607-14.

Nishizuka Y. Protein kinase C and lipid signaling for sustained cellular responses. *FASEB J* 1995;**9**:484-96.

O'Boyle NM, Banck M, James CA *et al*. Open Babel: An open chemial toolbox. *J Cheminform* 2011;**3**:33.

Ono Y, Fujii T, Igarashi K *et al*. Phorbol ester binding to protein kinase C requires a cysteine-rich zinc-finger-like sequence. *Proc Natl Acad Sci* 1989;**86**:4868-71.

Parikh JR, Doering WvE. Sulfur trioxide in the oxidation of alcohols by dimethyl sulfoxide. *J Am Chem Soc* 1967;**89**: 5505-7.

Peters MB, Yang Y, Wang B *et al*. Structural survey of zinc containing proteins and the development of the Zinc AMBER Force Field (ZAFF). *J Chem Theory Comput* 2010;**6**:2935-47.

Pettit GR, Herald CL, Doubek DL *et al*. Isolation and structure of bryostatin 1. *J Am Chem Soc* 1982;**104**:6846-8.

Philip M, Rowley DA, Schreiber H. Inflammation as a tumor promoter in cancer induction. *Semin Cancer Biol* 2004;**14**:433-9.

Russo P, Kisialiou A, Lamonaca P *et al*. New drugs from marine organisms in Alzheimer's disease. *Mar Drugs* 2016;**14**:5.

Sharkey NA, Blumberg PM. Highly lipophilic phorbol esters as inhibitors of specific [^{3}H]phorbol 12,13-dibutyrate binding. *Cancer Res* 1985;**45**:19-24.

Shimomura K, Mullinix MG, Kakunaga T *et al*. Bromine residue at hydrophilic region influences biological activity of aplysiatoxin, a tumor promoter. *Science* 1983;**222**:1242-4.

Shindo M, Irie K, Nakahara A *et al*. Toward the identification of selective modulators of protein kinase C (PKC) isozymes: establishment of a binding assay for PKC isozymes using synthetic C1 peptide receptors and identification of the critical residues involved in the phorbol ester binding. *Bioorg Med Chem* 2001;**9**:2073-81.

Steinberg SF. Structural basis of protein kinase C isoform function. *Physiol Rev* 2008;**88**:1341-78.

Suganuma M, Fujiki H, Tahira T *et al*. Estimation of tumor promoting activity and structure-function relationships of aplysiatoxins. *Carcinogenesis* 1984;**5**:315-8.

Szállási Z, Krsmanovic L, Blumberg PM. Nonpromoting 12-deoxyphorbol 13-esters inhibit phorbol 12-myristate 13-acetate induced tumor promotion in CD-1 mouse skin. *Cancer Res* 1993;**53**:2507-12.

Van der Spoel D, Lindahl E, Hess B *et al*. GROMACS: fast, flexible, and free. *J Comput Chem* 2005;**26**:1701-18.

Wan S, Knapp B, Wright DW *et al*. Rapid, precise, and reproducible prediction of peptide–MHC binding affinities from molecular dynamics that correlate well with experiment. *J Chem Theory Comput* 2015;**11**: 3346-56.

Yamori T, Matsunaga A, Sato S *et al*. Potent antitumor activity of MS-247, a novel DNA minor groove binder, evaluated by an *in vitro* and *in vivo* human cancer cell line panel. *Cancer Res* 1999;**59**:4042-9.